Chapter 5
Property Analysis

5.1 Introduction

In Chap. 4 the topic of matrix-reactance frequency converters mathematical modelling is discussed. The construction of a mathematical model is described, and analytical expressions are derived and evaluated. Using the mathematical description given by Eq. (4.24) the steady-state characteristics and time waveforms are obtained, whereas the transient states time waveforms are obtained from expression (4.23). The purpose of this chapter is to present these analytical results in easily understandable and readily usable graphical and tabular forms. The main objective is to provide a general appreciation of the practical significance of, and differences between, the external operating characteristics of the various MRFCs.

In this chapter, matrix-reactance frequency converters with balanced three-phase supply and load are considered. Also, it is assumed that the AC source has zero internal impedance. The circuit parameters are shown in Table 5.1. The properties of all topologies were examined for the same circuit parameters. Due to the large number of topologies, detailed extended results were shown only for the selected topology of MRFC-I-b-b. For this topology, the static characteristics for various load conditions and control parameters have been plotted. Furthermore, only for this topology is the transient state analysis presented. For other topologies, the basic static characteristics have been drawn. In the final part of this chapter, simulation studies of MRPC-I-b-b in the drive system with a cage asynchronous motor are presented. At the end of the chapter, a summary of the MRFCs properties, in tabular form and overall characteristics are presented. The practical implementation guidelines for the design of MRFCs are also depicted.

P. Szcześniak, *Three-Phase AC–AC Power Converters Based on Matrix Converter Topology*, Power Systems, DOI: 10.1007/978-1-4471-4896-8_5,

Table 5.1 Circuits parameters

Parameter	Symbol	Values
Supply voltage	U_S	230 V
Sfrequency of supply voltage	f	50 Hz
Source filter inductance	$L_{F1}, L_{F2}, L_{F3}, L_F$	1.5 mH
Input inductance	$L_{S1}, L_{S2}, L_{S3}, L_S$	1.5 mH
Output inductance	$L_{L1}, L_{L2}, L_{L3}, L_L$	1.5 mH
Resistance of source filter inductors	$R_{LF1}, R_{LF2}, R_{LF3}, R_{LF}$	0.01 Ω
Resistance of input inductors	$R_{LS1}, R_{LS2}, R_{LS3}, R_{LS}$	0.01 Ω
Resistance of output inductors	$R_{LL1}, R_{LL2}, R_{LL3}, R_{LL}$	0.01 Ω
Source filter capacitances	$C_{F1}, C_{F2}, C_{F3}, C_F$	10 μF
Input capacitances	$C_{S1}, C_{S2}, C_{S3}, C_S$	10 μF
Output capacitances	$C_{L1}, C_{L2}, C_{L3}, C_L$	10 μF
Resistance of loads	$R_{L1}, R_{L2}, R_{L3}, R_L$	60 Ω

5.2 Steady-State Analysis

Investigations that show the properties of the matrix-reactance frequency family of converters were carried out in a system consisting of the resistance load and the idealised power stage elements. Detailed results are shown only for MRFC-I-b-b topology (Fig. 3.7). The first step in the analysis of this circuit is to obtain the averaged output voltage waveforms (u_{L1}) for different setting frequencies $f_L = 25, 50$ and 75 Hz, that describe basic power-stage circuit operation—regulation of output voltage amplitude. These time waveforms are compiled in Fig. 5.1a, c, e. The waveforms of the output voltages were obtained using straightforward theoretical analysis techniques, based on the solution of Eq. (4.24), which for the analysed topology is given by (4.34) and (4.35). The presented output voltage waveforms are juxtaposed with source voltage u_{L1} time waveforms. The time waveforms shown in Fig. 5.1 confirm that by means of the discussed MRFC-I-b-b circuit frequency conversion and buck-boost load voltage changes are possible. For the $D_S = 0.75$ amplitude of output voltage u_{L1} is greater than the amplitude of source voltage u_{S1}. This theoretical output voltage agrees well with that obtained from real-time PSpice simulation, as is evident in Fig. 5.1b, d, f. Generally the results of the simulation experiment confirm the results of theoretical studies. Differences between analytic and simulation results are caused by higher harmonics being taking into account during the simulation experiment (non-stationary circuit).

To illustrate the effect of the discussed output voltage control, typical characteristics are shown with various sequence pulse duty factor D_S and setting output voltage frequency. Shown in Fig. 5.2 are the characteristics of voltage and current gain and input power factor as functions of load voltage setting frequency and pulse duty factor D_S, obtained by means of (4.24) and (4.33)–(4.35) for circuit parameters collected in Table 5.1. From these characteristics it is also visible that both a frequency conversion and a buck-boost load voltage change are possible. Using a simple control

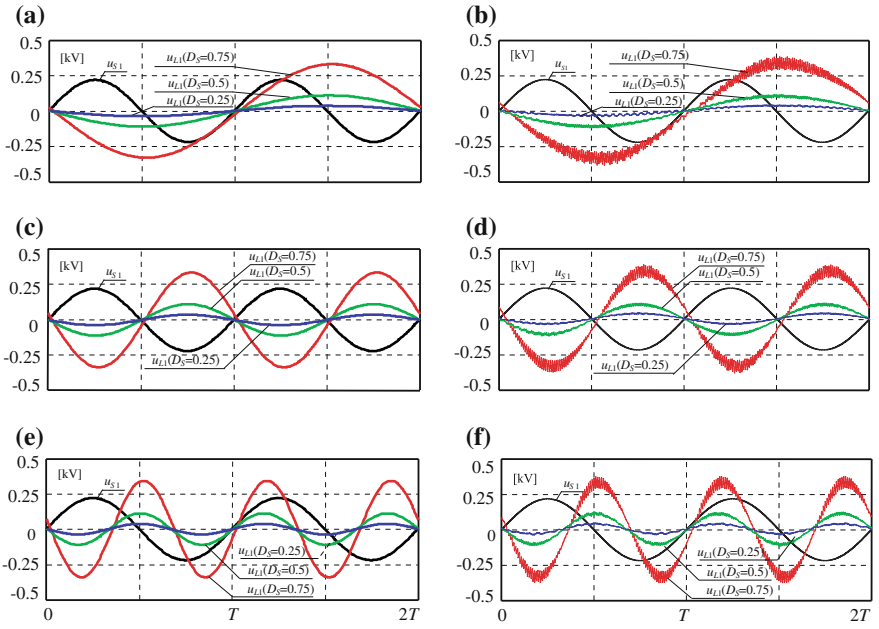

Fig. 5.1 Steady-state output voltage u_{L1} of MRFC-I-b-b for different sequence pulse duty factor D_S and setting output frequency: obtained by theoretical analysis **a** $f_L = 25\,\text{Hz}$, **c** $f_L = 50\,\text{Hz}$, **e** $f_L = 75\,\text{Hz}$: obtained by simulation, **b** $f_L = 25$ Hz, **d** $f_L = 50\,\text{Hz}$, **f** $f_L = 75\,\text{Hz}$

strategy, attributable to Venturini [11], for sequence pulse duty factor $D_S > c.a.$ 0.65 a load voltage greater than supply voltage can be obtained.

It can be seen from Fig. 5.2 that the frequency of output voltage has a significant effect on the converter properties. This chart clearly illustrates that the amplitude of output voltage for lower output frequency f_L is greater than the amplitude for the higher frequency (Fig. 5.2a). A similar influence of output setting frequency is visible on the characteristic of current gain (Fig. 5.2b) and input power factor λ_p (Fig. 5.2c). These visible differences are caused by the influence of the passive element parameters, which are used in the MRFC circuit. The MRFCs topologies are resonant *RLC* circuits. The influence of output voltage setting frequency on MRFC properties is presented in 3D form shown in Fig. 5.3.

The MRFC-I-b-b current input and output relations are nonlinear and strongly depend on the D_S factor, as shown in Figs. 5.2b and 5.3b. For the higher value of D_S (greater than 0.8) the input currents (i_{S1}, i_{S2}, i_{S3}) and source inductor currents (i_{LS1}, i_{LS2}, i_{LS3}) are much higher than for the lower value of D_S. The sample characteristic of current amplitudes in the discussed topology are presented in Fig. 5.4. By increasing the D_S ratio above 0.8, we take a large current from the source. Also, the amplitude of source inductor current is large. Inspection of Fig. 5.4 indicates that application of the discussed MRFC with high D_S is disadvantageous. In this case the magnetic saturation of the inductor cores can occur. The long-term magnetic

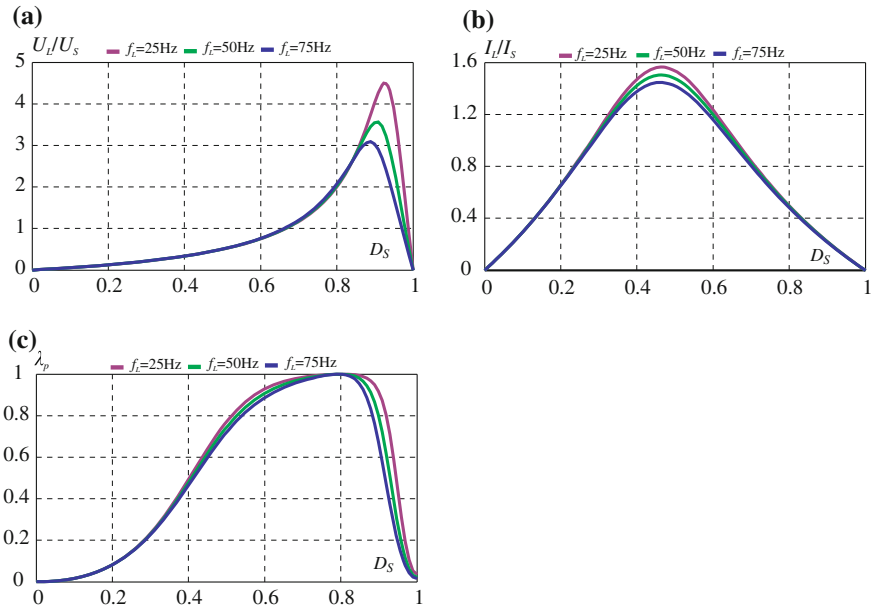

Fig. 5.2 Steady-state characteristics of MRFC-I-b-b: **a** voltage gain $K_U = \frac{U_L}{U_S}$, **b** current gain $K_I = \frac{I_L}{I_S}$, **c** input power factor λ_P

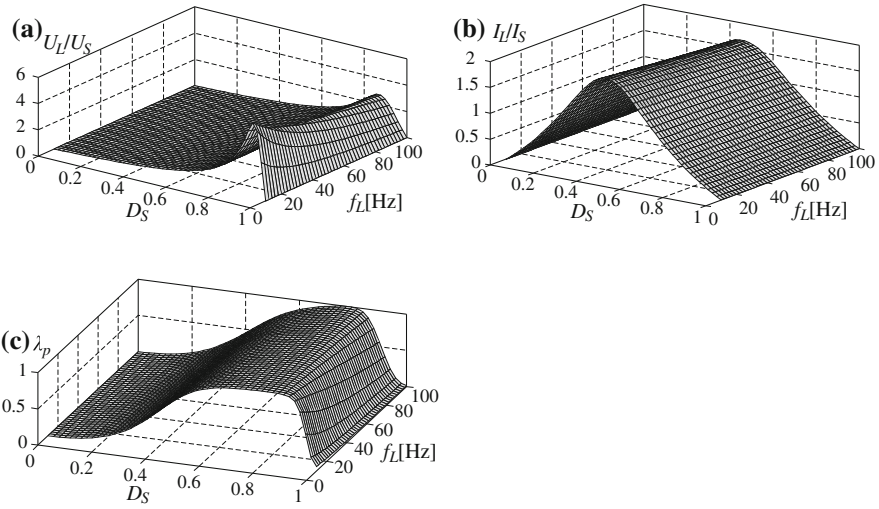

Fig. 5.3 Influence of load frequency on MRFC-I-b-b properties: **a** voltage gain K_U, **b** current gain K_I, **c** input power factor λ_P

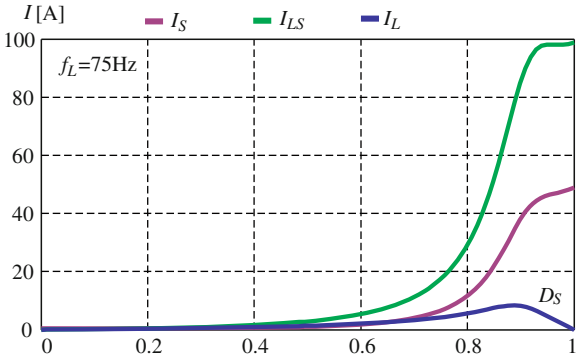

Fig. 5.4 Steady-state characteristic of current amplitudes in MRFC-I-b-b for $f_L = 25\,\text{Hz}$

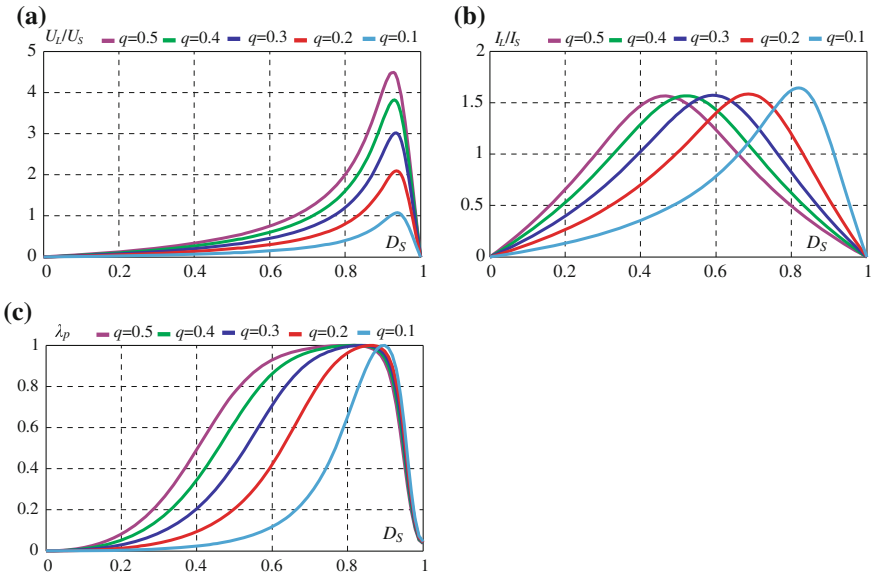

Fig. 5.5 Influence of coefficient q on MRFC-I-b-b properties for $f_L = 25\,\text{Hz}$: **a** voltage gain K_U, **b** current gain K_I, **c** input power factor λ_P

saturation of the cores usually leads to inductor or converter damage. The level of the inductor current must be taken into consideration in the design process.

As explained above, the output voltage waveform regulation is composed of two segments. The first is connected with the operation of matrix connected switches (S_{jK}) and the second with additional switches S_{L1}, S_{L2}, S_{L3}. In MRFC topologies there are two levels of output voltage regulation. There are additional degrees of control freedom. The first was presented previously and concerns modulation of sequence duty pulse D_S (Figs. 5.1, 5.2, 5.3 and 5.4). The second degree of control

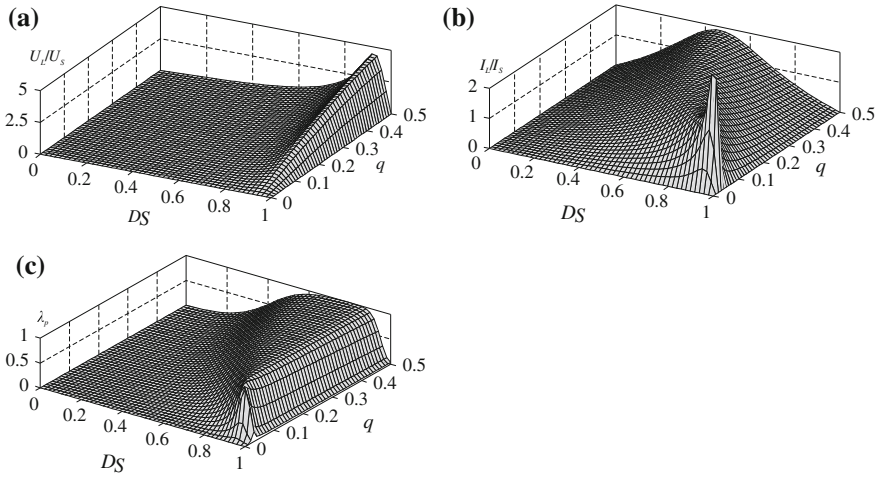

Fig. 5.6 Steady-state 3D characteristics of MRFC-I-b-b: **a** voltage gain K_U, **b** current gain K_I, **c** input power factor λ_P

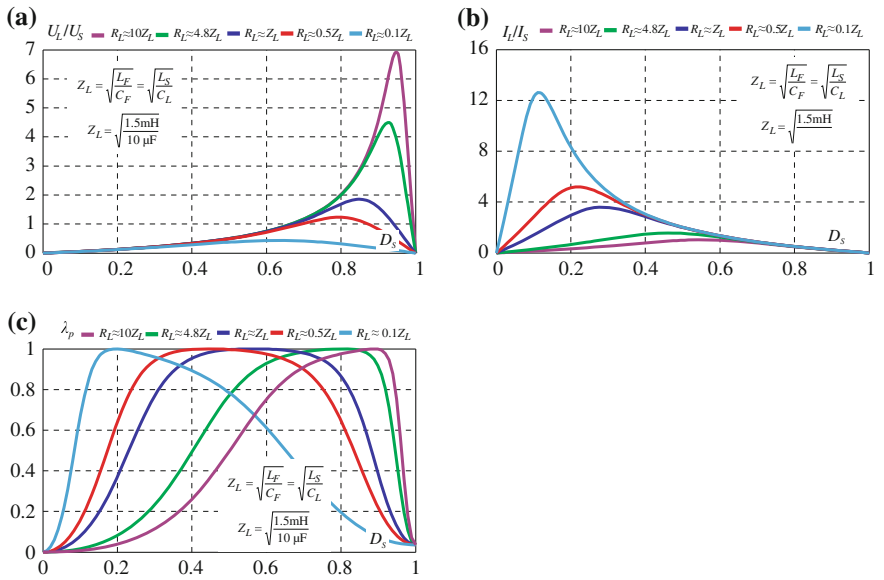

Fig. 5.7 Influence of load condition on MRFC-I-b-b properties for $f_L = 25\,\text{Hz}$: **a** voltage gain K_U, **b** current gain K_I, **c** input power factor λ_P

freedom of output voltage in MRFC is given by the variable of matrix voltage gain q. Coefficient q is defined as a setting quotient of output and input voltages on matrix switches. All time waveforms and static characteristic from Figs. 5.1, 5.2, 5.3 and 5.4 are presented with optimum value of coefficient $q = 0.5$ (optimum for Venturini control strategy). Figure 5.5 shows the variation in the MRFC-I-b-b

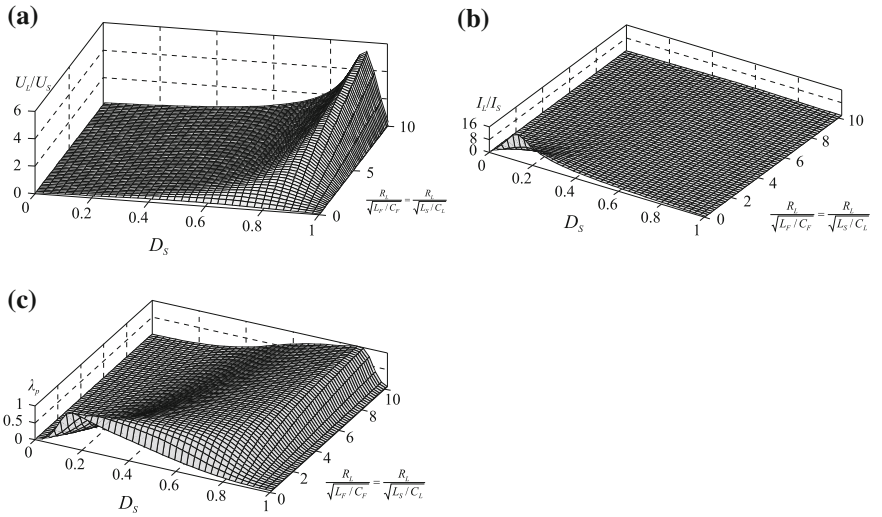

Fig. 5.8 Influence of condition load on MRFC-I-b-b properties for $f_L = 25$ -3D characteristics: **a** voltage gain K_U, **b** current gain K_I, **c** input power factor λ_P

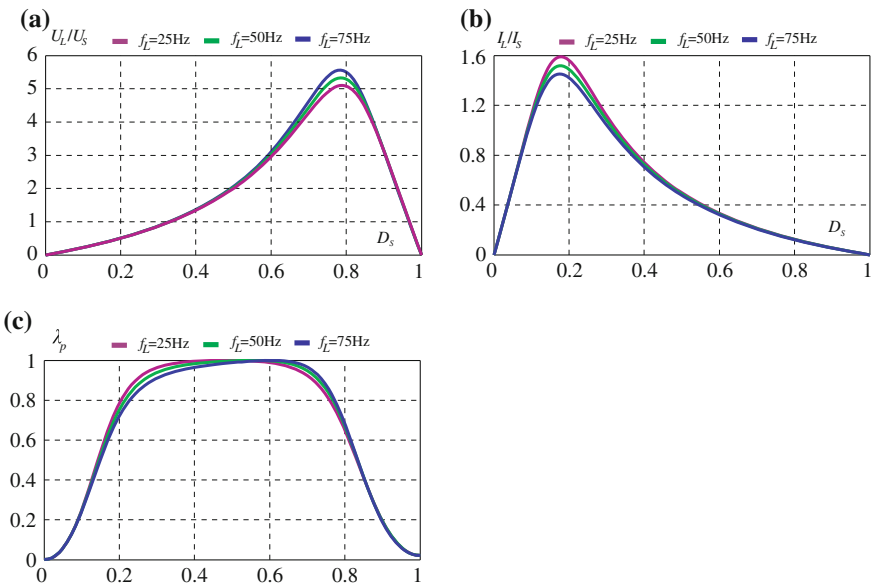

Fig. 5.9 Steady-state characteristics of MRFC-II-b-b: **a** voltage gain K_U, **b** current gain K_I, **c** input power factor λ_P

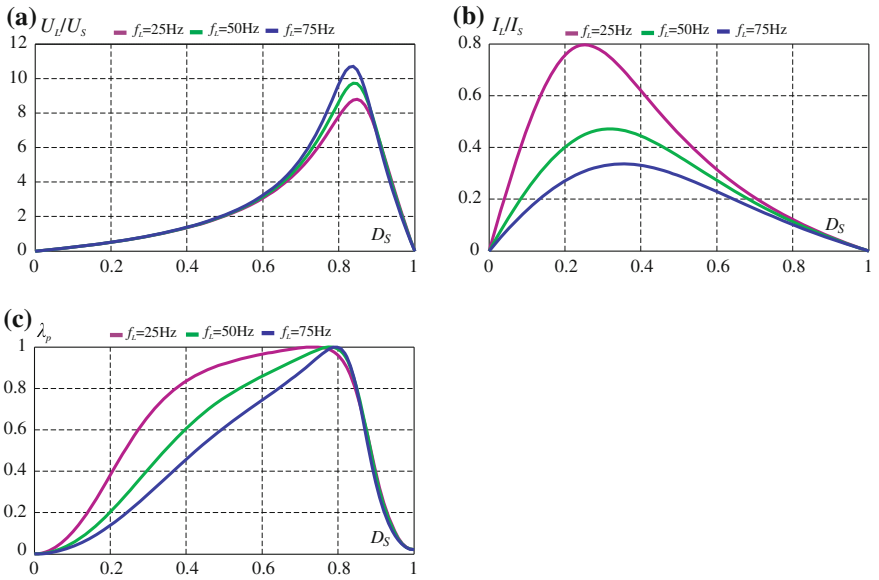

Fig. 5.10 Steady-state characteristics of MRFC-I-c: **a** voltage gain K_U, **b** current gain K_I, **c** input power factor λ_P

properties for a different value of q as a function of sequence pulse duty factor D_S. All the possibilities of output voltage control are presented in 3D characteristics in Fig. 5.6. In this figure, the two levels of control with q and D_S variations are presented. The additional degree of control freedom provided by the coefficient q can be beneficial for MRFCs control properties.

The MRFC is equivalent to an *RLC* resonant circuit whose values are varied by the load character. Furthermore, the MRFC transfers energy from sources to the load, along with their properties, such as in transmission lines. These types of systems are characterised by characteristic impedance Z_{Ch}. Thus, maximum transfer of power from the source to the load takes place when the load is matched to the source. The parameters of MRFC-I-b-b circuits and characteristic impedance Z_{Ch} are related as follows [1]:

$$Z_{Ch} = \sqrt{\frac{L_F}{C_F}} = \sqrt{\frac{L_S}{C_L}}. \tag{5.1}$$

The full load-matching condition is achievable if:

$$Z_{Ch} = \underline{Z}_L = R_L. \tag{5.2}$$

Efficient power transfer is possible with other converter and load impedances, but with less capacity. In addition to the problem of matching a purely resistive load that is not equal to Z_{Ch}, a typical practical problem includes substantial load reactance as well. Figure 5.7 shows the influence of load conditions on MRFC-I-b-b

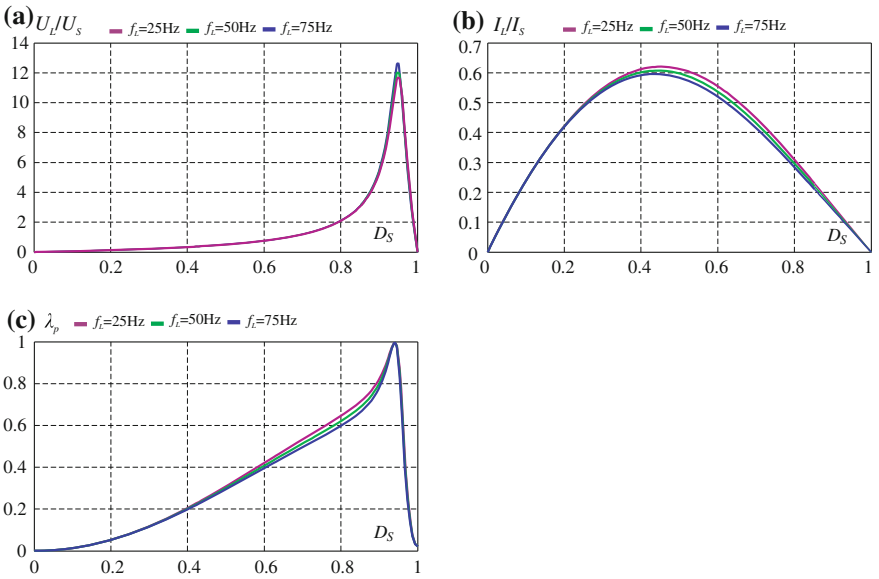

Fig. 5.11 Steady-state characteristics of MRFC-II-c: **a** voltage gain K_U, **b** current gain K_I, **c** input power factor λ_P

properties. The analysed MRFC is sensitive to changes in the load parameters. In this book only the resistance load condition is analysed. For load resistance equal to or greater than the characteristic impedance ($R_L \geq Z_{Ch}$) a voltage transfer ratio greater than one is achieved. In the case when $R_L \leq Z_{Ch}$, the output voltage is less than source voltage. Thus in the load-matched case there are minimum power losses and maximum efficiency. The 3D chart of Fig. 5.8 shows in detail the analysis converter's sensitivity of parameters to load conditions.

All the results presented in Figs. 5.7 and 5.8 show the limits of load variation. These limits are the reason that MRFCs have a potential application as a universal frequency converter. The relationship of MRFCs *LC* components and load conditions should be individually selected depending on the type of load.

The presented steady-state time waveforms and characteristics concern the MRFC-I-b-b topology. Other topologies of MRFCs have similar properties to the MRFC-I-b-b. The setting load frequency and load conditions, too, have an influence on output voltages and the input power factor. Similarly, two degrees of control freedom are given, with variations of q and D_S coefficients. However, the static characteristics are different. For the other topologies only basic static characteristics are indicated, showing the relations of voltage, current gain and input power factor as a function of D_S for three output frequencies $f_L - 25, 50, 75$ Hz.

Analytical characteristics for MRFC-II-b-b were obtained using theoretical analysis techniques, based on the solution of Eq. (4.24), in the form presented in Table 4.1. Figure 5.9 illustrates the obtained results. It can be seen that the obtained voltage

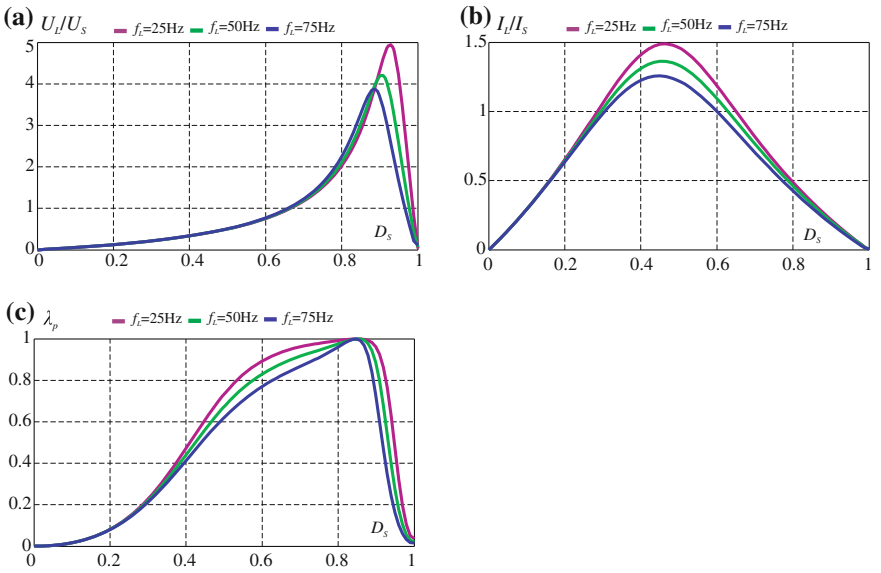

Fig. 5.12 Steady state characteristics of MRFC-I-z: **a** voltage gain K_U, **b** current gain K_I, **c** input power factor λ_P

gain for MRFC-II-b-b is greater than the voltage gain for MRFC-I-b-b. Also, the performance of the input power factor is better. In practical applications, when voltage gain of a little larger than one is needed a detailed analysis and design procedure is required. In this topology smaller capacitances and inductor can be applied.

Similar characteristics are presented for MRFC-I-c (Fig. 5.10) and MRFC-II-c (Fig. 5.11). The average stationary equations are included in the Tables 4.2 and 4.3 for MRFC-I-c and MRFC-II-c, respectively. To illustrate the properties of Zeta MRFC topologies similar results are presented in Figs. 5.12 and 5.13 for MRFC-I-z and MRFC-II-z, respectively. The mathematical models for these topologies are presented in Tables 4.4 and 4.5.

The graphs in Figs. 5.14 and 5.15 correspond to steady-state operation in SEPIC MRFC topologies, and were obtained from expressions included in Tables 4.6 and 4.7. The last plot in Fig. 5.16 shows the MRFC-b properties in a steady state. The boost MRFC averaged model is presented in Table 4.8.

The concluding part of the chapter is concerned with the summary of properties of all MRFCs. The overall characteristics and tabular comparison are presented. The practical implementation guidelines for the design of MRFCs are also outlined in the summary of the chapter.

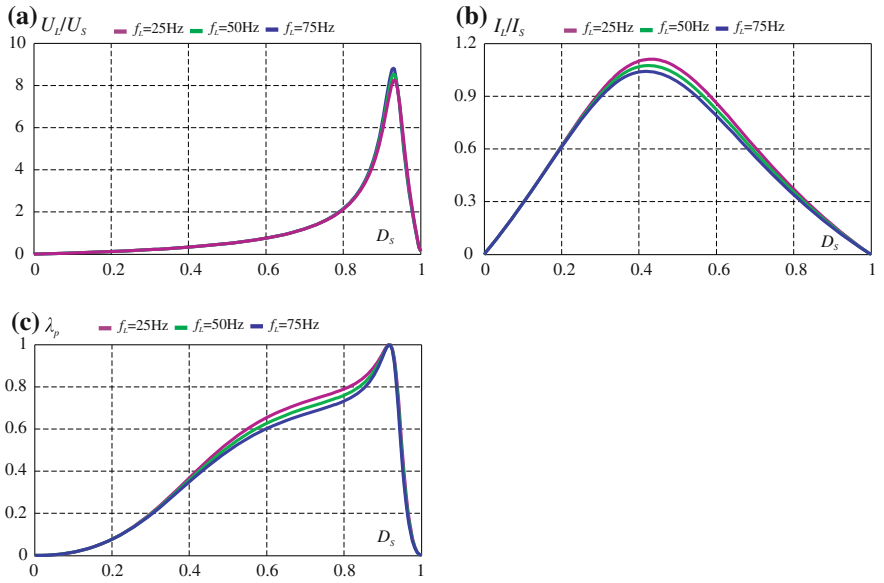

Fig. 5.13 Steady-state characteristics of MRFC-II-z: **a** voltage gain K_U, **b** current gain K_I, **c** input power factor λ_P

5.3 Transient State Analysis

The performance of an MRFC is studied in terms of steady-state and transient-state analysis. The steady-state analysis is important for selecting the converter operating conditions, ensuring the optimum working conditions for a particular application and for a given configuration of load and power supply. The transient-state analysis of an MRFC is vital for assessing the dynamics of the system and disturbances generated during transients as well as to develop a protection strategy. The transient simulations presented in the literature are used in two main groups of analyses: transient analysis for step changes of control signals and power stage parameters. The models developed for transient stability analysis are generally valid in longer time frames.

These studies are focused on the converter analysis of step change in control signals, such as the sequence pulse duty factor D_S and setting load frequency f_L. Furthermore, the supply voltage changes will be analysed. Using the mathematical description given by Eq. (4.23) the transient state time waveforms are obtained. Similarly, as in the above subchapter only MRFC-I-b-b topology was analysed.

In Figs. 5.17 and 5.18 are shown exemplary voltage and current time waveforms illustrating the selected cases of the transient states in the discussed MRFC. Figure 5.17 depicts the theoretical transient responses of state variables at a step change of the sequence pulse duty factor D_S from 0.5 to 0.7 for output frequencies $f_L = 25\,\text{Hz}$. The responses of state variables at a step change in the supply voltages

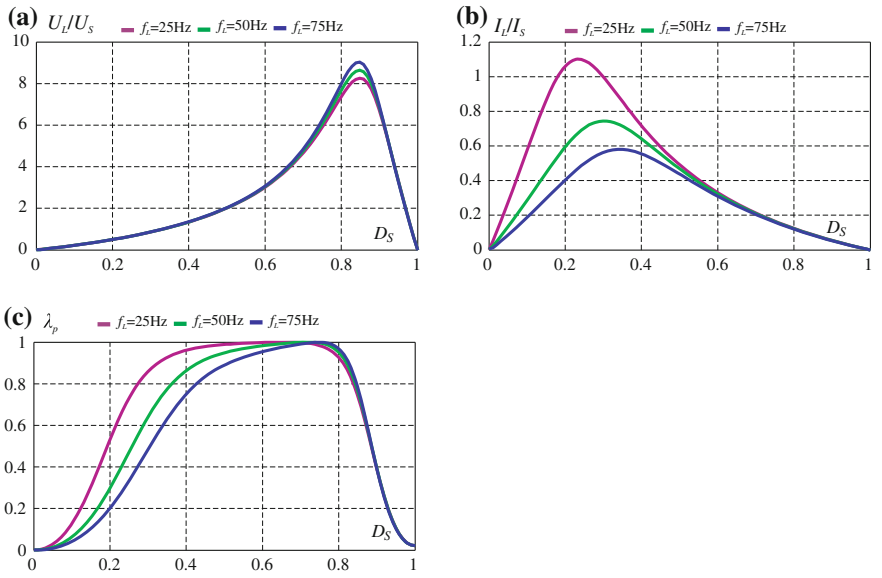

Fig. 5.14 Steady-state characteristics of MRFC-I-s: **a** voltage gain K_U, **b** current gain K_I, **c** input power factor λ_P

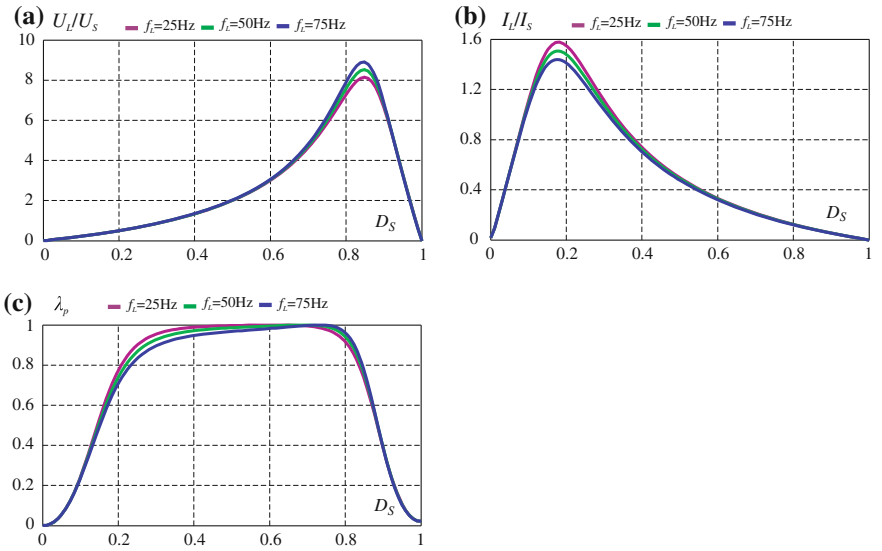

Fig. 5.15 Steady-state characteristics of MRFC-II-s: **a** voltage gain K_U, **b** current gain K_I, **c** input power factor λ_P

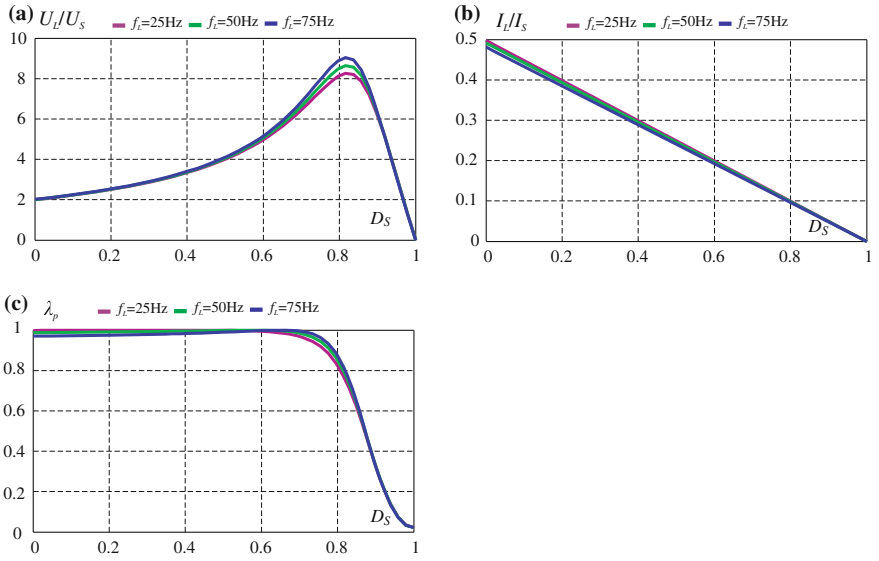

Fig. 5.16 Steady-state characteristics of MRFC-b: **a** voltage gain K_U, **b** current gain K_I, **c** input power factor λ_P

U_{Sm} from 150 to 230 V for output frequencies $f_L = 25$ Hz at $D_S = 0.75$, can be observed in Fig. 5.18.

The waveforms in Figs. 5.17 and 5.18 confirm good dynamic properties of such a converter. The converter transient response is relatively short. In the case of a step change in coefficient D_S, the transient period is approximately equal to 0.25 times the supply voltage period, but the current distortion has a longer time response. There are high frequency oscillations which last approximately to three periods of this current, and afterwards the system attains steady-state condition. In the second case the time response is also short. The main distortion lasts about 0.5 times to period of source voltage, but the high frequency oscillations last more than 4 periods.

To verify the averaged modelling accuracy, Fig. 5.19 shows the state variables' waveforms during the transience. The waveforms obtained by switched-circuit transient PSpice simulation are shown together with the waveforms obtained by analysis of the averaged model (4.23). As shown in Fig. 5.19 the calculation and simulation test results demonstrate good correlation which confirms the usefulness of the used analytical averaged method.

The properties of other MRFCs in transient state are not presented in this book. Some results can be found in [2–5, 8, 9].

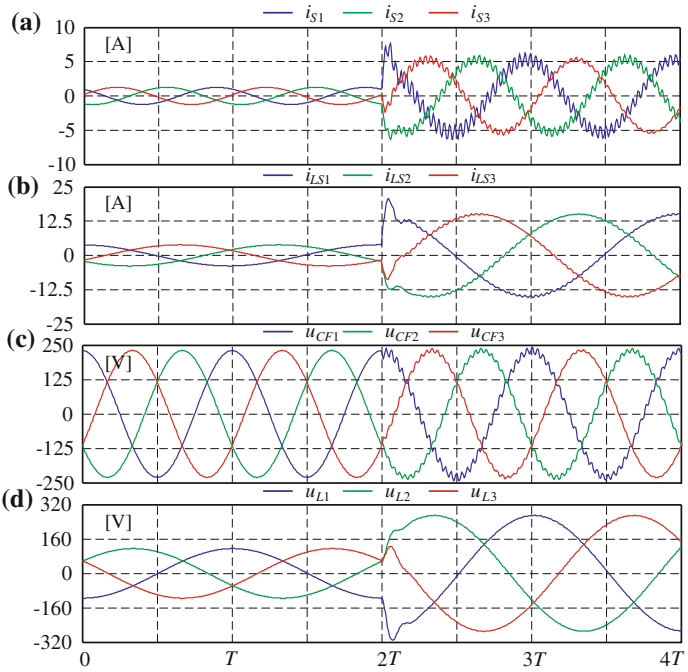

Fig. 5.17 Transient responses of states variables at step change in the sequence pulse duty factor D_S from 0.5 to 0.7, for $f_L = 25\,\text{Hz}$

5.4 Drive System Application

As an exemplary application of the MRFC devices shown above an application in a power electric drive system with induction cage motor is shown (Fig. 5.20). Simulation of a drive system with an MRFC and cage asynchronous motor has been carried out with the help of the PSpice computer program. A cage motor simulation model was constructed in PSpice based on mathematical relations (5.3)–(5.14) [6], which describe the motor operation in a coordinate system rotating with an angular speed ω, called the coordinate system $\alpha\beta\gamma$.

$$u_{s\alpha} = R_s i_{s\alpha} + \frac{\omega(\psi_{s\gamma} - \psi_{s\beta})}{\sqrt{3}} + \frac{d\psi_{s\alpha}}{dt}, \tag{5.3}$$

$$u_{s\beta} = R_s i_{s\beta} + \frac{\omega(\psi_{s\alpha} - \psi_{s\gamma})}{\sqrt{3}} + \frac{d\psi_{s\beta}}{dt}, \tag{5.4}$$

$$u_{s\gamma} = R_s i_{s\gamma} + \frac{\omega(\psi_{s\beta} - \psi_{s\alpha})}{\sqrt{3}} + \frac{d\psi_{s\gamma}}{dt}, \tag{5.5}$$

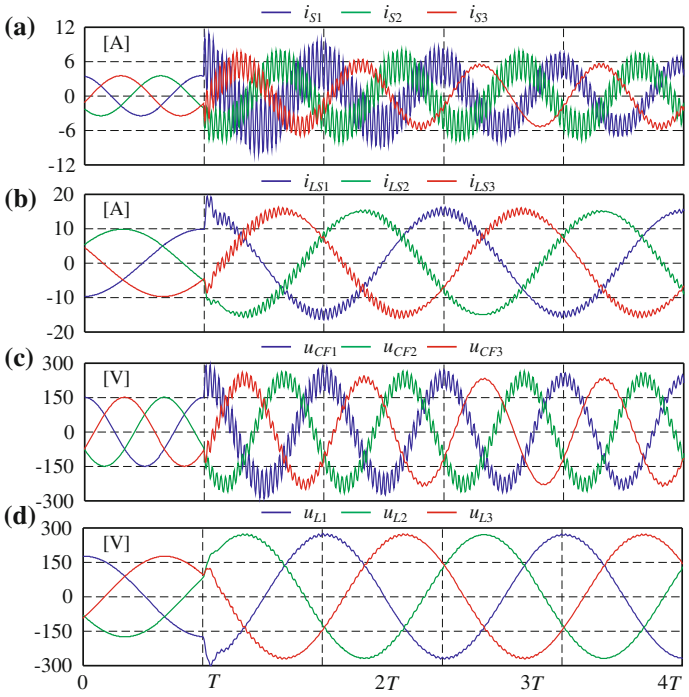

Fig. 5.18 Transient responses of state variables at step change in the supply voltage U_{Sm} from 150 to 230 V, for $f_L = 25$ Hz at $D_S = 0.75$

$$u'_{r\alpha} = R'_r i'_{r\alpha} + (\omega - \omega_r)\frac{(\psi'_{r\gamma} - \psi'_{r\beta})}{\sqrt{3}} + \frac{d\psi'_{r\alpha}}{dt}, \tag{5.6}$$

$$u'_{r\beta} = R'_r i'_{r\beta} + (\omega - \omega_r)\frac{(\psi'_{r\alpha} - \psi'_{r\gamma})}{\sqrt{3}} + \frac{d\psi'_{r\beta}}{dt}, \tag{5.7}$$

$$u'_{r\gamma} = R'_r i'_{r\gamma} + (\omega - \omega_r)\frac{(\psi'_{r\beta} - \psi'_{r\alpha})}{\sqrt{3}} + \frac{d\psi'_{r\gamma}}{dt}, \tag{5.8}$$

$$\psi_{s\alpha} = L_{sl} i_{s\alpha} + M(i_{s\alpha} - i'_{r\alpha}), \tag{5.9}$$

$$\psi_{s\beta} = L_{sl} i_{s\beta} + M(i_{s\beta} - i'_{r\beta}), \tag{5.10}$$

$$\psi_{s\gamma} = L_{sl} i_{s\gamma} + M(i_{s\gamma} - i'_{r\gamma}), \tag{5.11}$$

$$\psi'_{r\alpha} = L'_{rl} i'_{r\alpha} + M(i_{s\alpha} - i'_{r\alpha}), \tag{5.12}$$

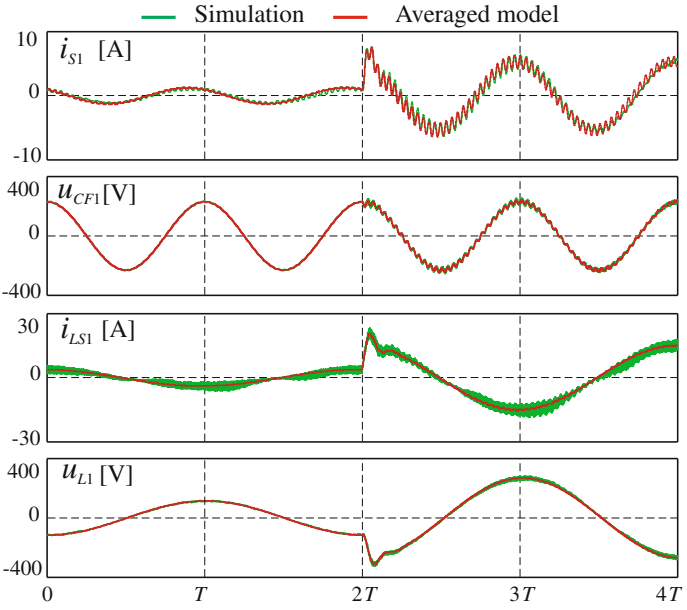

Fig. 5.19 Comparison of PSpice simulation and averaged model results from transient responses of state variables at step change in the sequence pulse duty factor D_S from 0.5 to 0.7, $f_L = 25\,\text{Hz}$

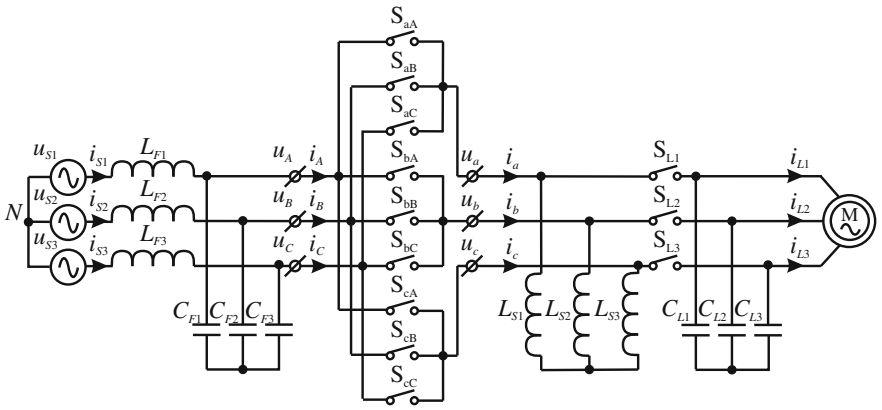

Fig. 5.20 Drive system with MRFC-I-b-b and induction cage motor

$$\psi'_{r\beta} = L'_{sl} i'_{r\beta} + M(i_{s\beta} - i'_{r\beta}), \tag{5.13}$$

$$\psi'_{r\gamma} = L'_{rl} i'_{r\gamma} + M(i_{s\gamma} - i'_{r\gamma}), \tag{5.14}$$

where: $u_{s\alpha}$, $u_{s\beta}$, $u_{s\gamma}$, $i_{s\alpha}$, $i_{s\beta}$, $i_{s\gamma}$—stator voltages and currents that are described in $\alpha\beta\gamma$ coordinates rotating with an angular speed ω; $u'_{r\alpha}$, $u'_{r\beta}$, $u'_{r\gamma}$, $i'_{r\alpha}$, $i'_{r\beta}$, $i'_{r\gamma}$ - rotor

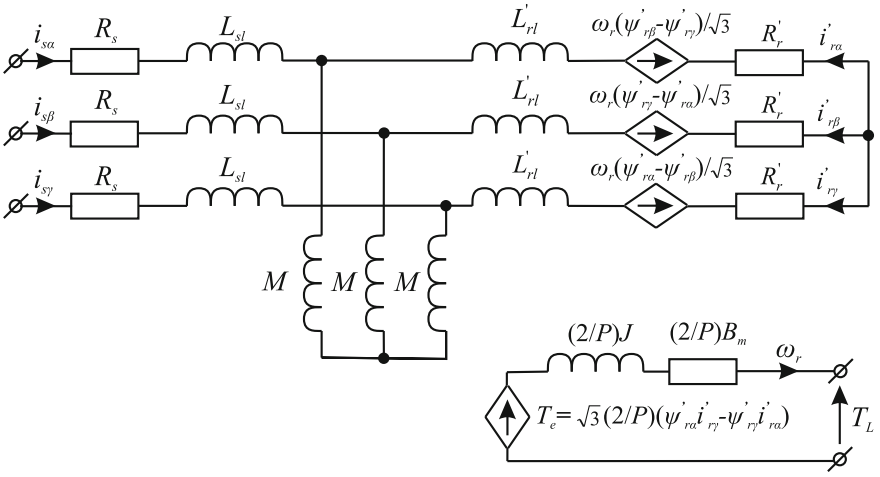

Fig. 5.21 Simplified model of cage induction motor described in $\alpha\beta\gamma$ coordinate

voltages and currents that are described in $\alpha\beta\gamma$ coordinates rotating with an angular speed ω which are reduced to stator coordinate; R_s, R_r—stator and rotor resistances; L_{sl}, L_{rl}—leakage inductance of stator and rotor windings; $M = \frac{3}{2}L_{ms}$—magnetising inductance; L_{ms}—magnetising inductance of the stator winding; $\psi_{s\alpha}$, $\psi_{s\beta}$, $\psi_{s\gamma}$—rotor flux described in $\alpha\beta\gamma$ coordinates; $\psi'_{r\alpha}$, $\psi'_{r\beta}$, $\psi'_{r\gamma}$—stator flux described in $\alpha\beta\gamma$ coordinates which are reduced to stator coordinates.

The mechanical system is described by the following equation [6]:

$$T_e = \frac{2}{P}J\omega_r + \frac{2}{P}B_m\omega_r + T_L, \tag{5.15}$$

where: T_e—electromagnetic torque; P—number of pole pairs; J—moment of inertia of the mechanical system; ω_r—rotor angular speed; T_L—load moment; B_m—viscous friction coefficient. Electromagnetic torque can also be represented by the following equation [6]:

$$T_e = \sqrt{3}\frac{P}{2}(\psi'_{r\alpha}i'_{r\gamma} - \psi'_{r\gamma}i'_{r\alpha}) \tag{5.16}$$

Equations (5.15) and (5.16) are implemented in the simulation model to approximate the mechanical parameters of the system and the loading conditions. For the induction machine fed from the stator circuit the rotation speed in $\alpha\beta\gamma$ coordinate is set by zero $\omega = 0$. Then, a simplified model of the cage induction motor determined by Eqs. (5.3)–(5.16) are presented in Fig. 5.21 [6].

A computer simulation was carried out using the simulation parameters of the inverter and the motor put together in Table 5.2 [7, 8]. The simulation results of a drive system with MRFC-I-b-b topology can be observed in 5.22–5.24. In Figs. 5.22 and 5.23 are presented the exemplary time waveforms of converter input and output

Table 5.2 Simulation parameters of drive system with MRFC-I-b-b

Parameter	Symbol	Value
Supply voltage	U_S	230 V
Frequency of supply voltage	f	50 Hz
Switching frequency	f_S	5 kHz
Maximum simulation step	t_p	1 μs
Source filter inductance	L_{F1}, L_{F2}, L_{F3}	0.5 mH
Source inductance	L_{S1}, L_{S2}, L_{S3}	0.5 mH
Source filter capacitance	C_{F1}, C_{F2}, C_{F3}	20 μF
Load capacitance	C_{L1}, C_{L2}, C_{L3}	20 μF
Motor power	P_n	2.2 kW
Switch resistance in turn-on state	R_{ON}	0.01 Ω
Switch resistance in turn-off state	R_{OFF}	0.1 MΩ
Stator and rotor resistance	R_s, R'_r	2.5002 Ω
Leakage inductance of stator and rotor windings	L_{sl}, L'_{rl}	0.011 H
Magnetizing inductance	M	0.4576 H
Moment of inertia	J	0.06825 kg m^2
Viscous friction coefficient	B_m	1.024 10^{-3}
Number of pole pairs	P	4

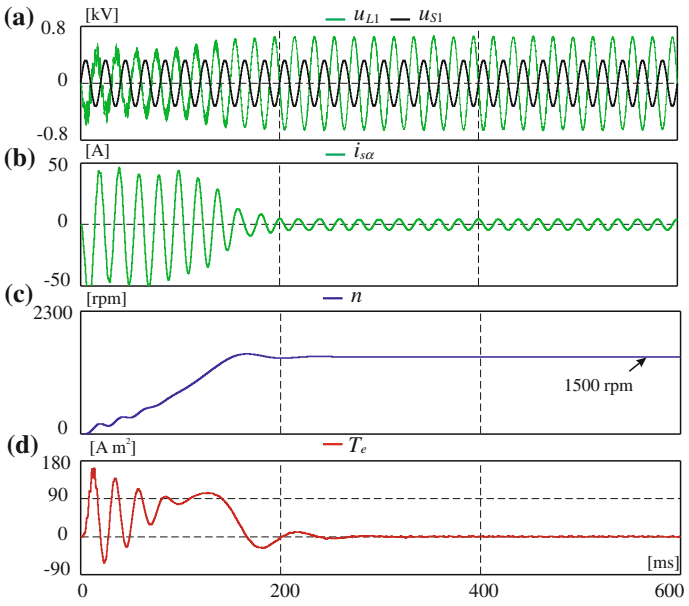

Fig. 5.22 Simulation time waveforms of drive system with MRFC-I-b-b during motor starting, for $f_L = 50$ Hz, $D_S = 0.8$, $q = 0.5$: **a** input (u_{S1}) and output (u_{L1}) voltage of converter, **b** motor current ($i_{S\alpha}$), **c** speed (n), **d** electromagnetic torque (T_e)

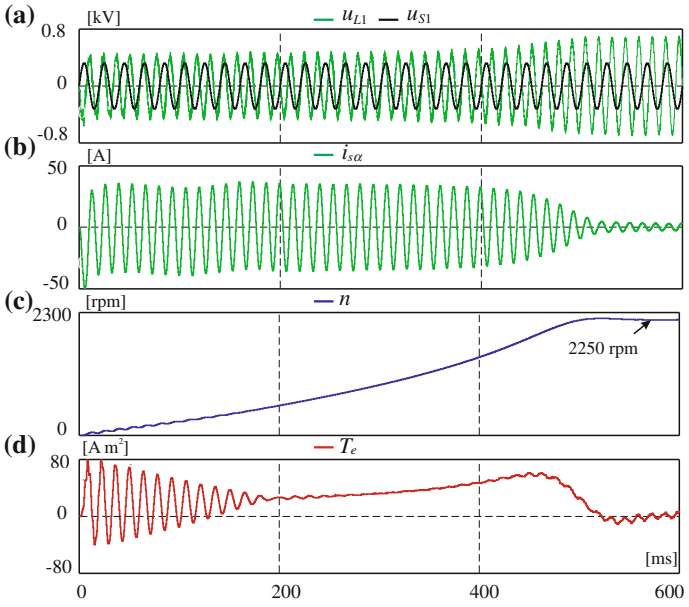

Fig. 5.23 Simulation time waveforms of drive system with MRFC-I-b-b during motor starting, for $f_L = 75\,\text{Hz}$, $D_S = 0.8$, $q = 0.5$: **a** input (u_{S1}) and output (u_{L1}) voltage of converter, **b** motor current ($i_{S\alpha}$), **c** speed (n), **d** electromagnetic torque (T_e)

voltage (u_{S1}, u_{L1}), motor current ($i_{S\alpha}$), speed (n) and electromagnetic torque, during the motor starting for output voltage frequency $f_L = 50$ and 75 Hz. Whereas, in Fig. 5.24 the same time waveforms are presented in motor start and reverse states for output voltage frequency $f_L = 50\,\text{Hz}$. All results are obtained for open loop control for sequence duty factor $D_S = 0.8$ [7, 8].

All these results show that the converter voltage (u_{L1}) is greater than the supply voltages (Figs. 5.22a, 5.23a, 5.24a). This results in a faster motor start-up to the nominal speed than direct motor attached to the supply grid (Figs. 5.22c, 5.23c, 5.24c). As is clear from (Figs. 5.22b, 5.23b, 5.24b) during the start-up process and reverse process the stator currents $i_{S\alpha}$ are greater than in steady state. Increased motor power consumption in transient states causes a drop in the MRFC output voltage (u_{L1}). This voltage is fixed after reaching the nominal motor speed $n_{(f_L)}$ for a given frequency of motor supply voltage (f_L). It should be noted that MRFC output voltage is greater than the supply voltage at any time Table 5.2 [7, 8]. In practical solutions of drive systems with a feedback control the output voltage can be maintained at a constant level equal to or greater than the supply voltage. Figures 5.22, 5.23 and 5.24 illustrate that the motor supply voltages have a sinusoidal shape. This property is an advantage of using an MRFC in a drive system.

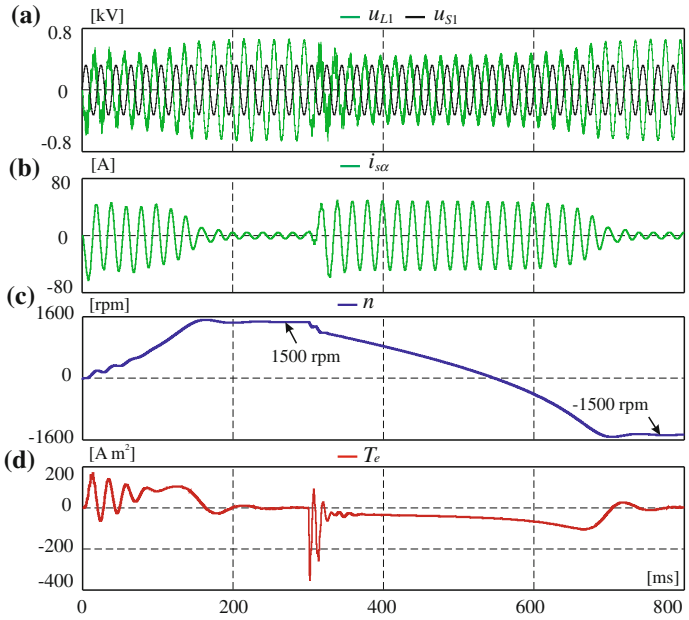

Fig. 5.24 Simulation time waveforms of drive system with MRFC-I-b-b during motor starting and revers, for $f_L = 50\,\text{Hz}$, $D_S = 0.8$, $q = 0.5$: **a** input (u_{S1}) and output (u_{L1}) voltage of converter, **b** motor current ($i_{S\alpha}$), **c** speed (n), **d** electromagnetic torque (T_e)

5.5 Chapter Summary

This chapter presented the basic steady and transient states theoretical results of MRFCs. Due to the large number of converters, only the MRFC-I-b-b topology has been analysed in detail. The theoretical results presented in this chapter, and the exact match between theoretical analysis and numerical simulation that has been achieved, indicate the correctness of the theoretical analysis.

For final comparison of all topologies, the static characteristics of voltage and current gain and input power factor for $f_L = 25\,\text{Hz}$ are demonstrated in Fig. 5.25 [2, 8].

In all the analysed topologies of MRFCs, for modified Venturini control strategy and parameters listed in Table 5.1, it is possible to obtain a voltage gain greater than unity as shown in Fig. 5.25a. The voltage gain, depending on the topology, varies widely in range, and the maximum is over 10 for the MRFC-II-c topology. The level of reactor currents in the selected topology can be analysed based on the current gain characteristic (Fig. 5.25b). Figure 5.25c shows the input power factor of the whole family of MRFCs using a modified Venturini control strategy. In converters with this modulation strategy it is not possible to control the input power factor. The modification of the control strategy is needed for input power factor improvement.

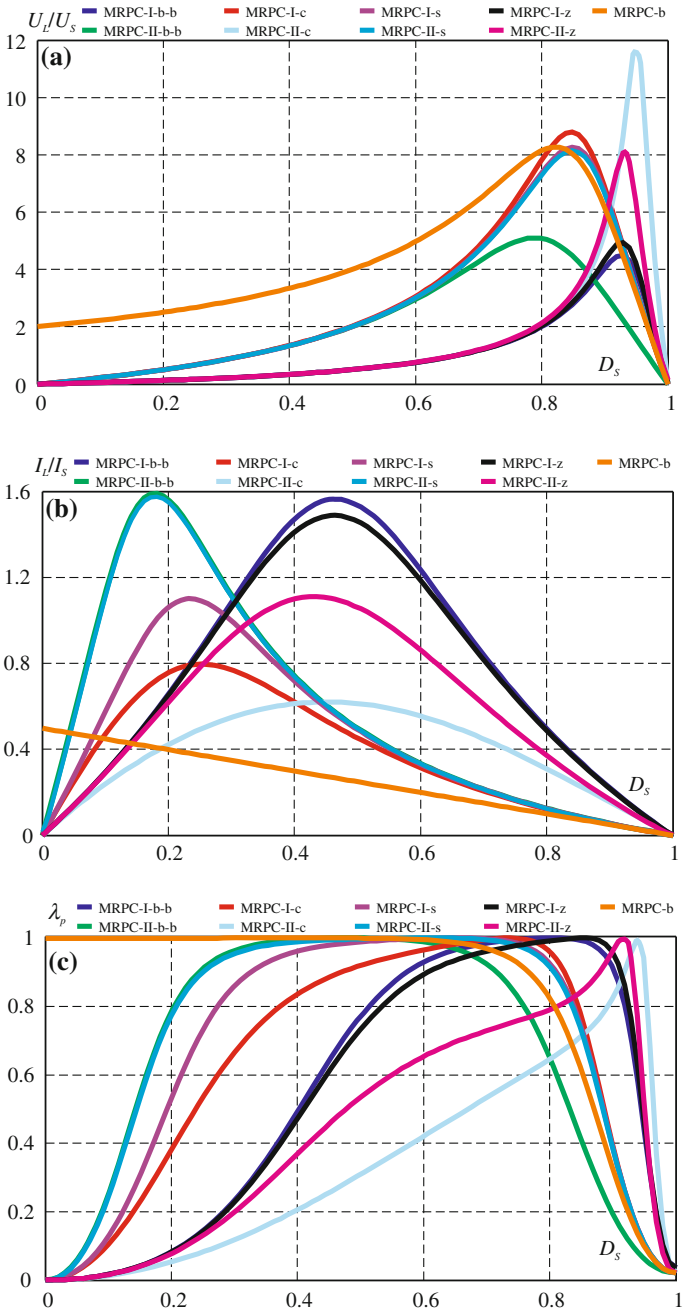

Fig. 5.25 Comparison of static characteristics of: **a** voltage gain K_U, **b** current gain K_I, **c** input power factor λ_P

Table 5.3 Summaries of the maximum voltage gain and input power factor of MRFCs

Topology	Maximum voltage gain			Range D_S, when $\lambda_p > 0.95$		
	$f_L = 25\,\text{Hz}$	$f_L = 50\,\text{Hz}$	$f_L = 75\,\text{Hz}$	$f_L = 25\,\text{Hz}$	$f_L = 50\,\text{Hz}$	$f_L = 75\,\text{Hz}$
MRPC-I-b-b	4,49	3.56	3.09	0.62–0.87	0.65–0.85	0.67–0.85
MRPC-II-b-b	5.10	5.32	5.55	0.28–0.66	0.34–0.69	0.36–0.70
MRPC-I-c	8.78	9.73	10.70	0.56–0.79	0.70–0.81	0.74–0.81
MRPC-II-c	11.68	11.98	12.42	0.93–0.94	0.93–0.94	0.93–0.94
MRPC-I-z	4.94	4.19	3.86	0.67–0.89	0.76–0.87	0.79–0.86
MRPC-II-z	8.24	8.54	8.80	0.89–0.92	0.90–0.92	0.90–0.92
MRPC-I-s	8.26	8.64	9.03	0.38–0.77	0.5–0.79	0.59–0.80
MRPC-II-s	8.14	8.52	8.90	0.30–0.77	0.34–0.78	0.41–0.79
MRPC-b	8.25	8.64	9.04	0.00–0.71	0.00–0.73	0.00–0.75

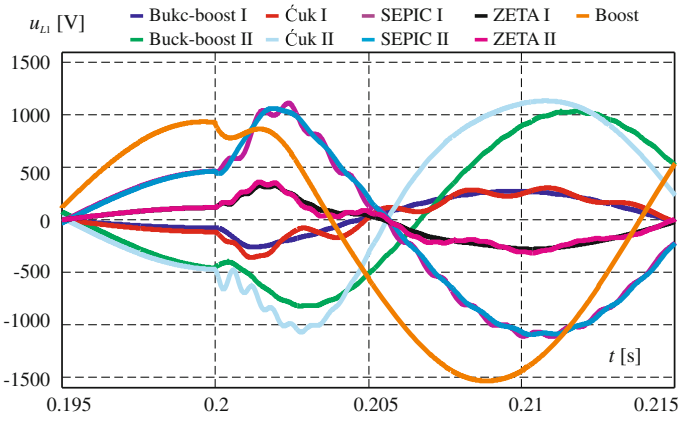

Fig. 5.26 Transient responses of output voltages of MRFCs at step change of the sequence pulse duty factor D_S from 0.5 to 0.7, for $f_L = 25\,\text{Hz}$

Using SVM technique for MRFC control the improvement of their properties is possible [10].

Table 5.3 summarises the maximum voltage gain and input power factor range of slightly less than unity for all MRFCs with modified Venturini control strategy and parameters in Table 5.1 [8]. From this table it can also be seen that there is significant difference between the MRFC topologies.

Moreover, in order to compare the dynamic properties of the whole family of MRFCs, the output voltage time waveforms in transient states for D_S changes from 0.5 to 0.7 for $f_L = 25\,\text{Hz}$ are presented in Fig. 5.26. The time response depends on the topology and the voltage gain for the initial steady state [2, 8].

During the practical implementation and design of the selected MRFC topology the type of load, the maximum voltage gain and the switching frequency of power switches should be considered. In addition, the design of reactors must take into account their current values. To estimate the level of currents, the characteristics of current gain may be useful.

Based on the Obtained Results it can be Concluded that

- MRFCs allow a change of the output voltage frequency and the buck-boost output voltage regulation,
- there are two degrees of control freedom in the output voltage through the coefficient q and sequence pulse duty factor D_S,
- properties of MRFCs depends on the setting frequency of the output voltage,
- properties of MRFCs are sensitive to load changes,
- systems with MRPCs have good dynamic properties,
- in MRFCs with modified Venturini control strategy the input power factor regulation is not possible,
- in design process of MRFCs experimental setup the maximum voltage gain, current level and switching frequency must be taken into account.

References

1. Fedyczak Z (2003) PWM AC voltage transforming circuits (In Polish). Zielona Góra University Press, Zielona Góra
2. Fedyczak Z, Szcześniak P (2012) Matrix-reactance frequency converters using an low frequency transfer matrix modulation method. Electr Power Syst Res 83(1):91–103
3. Fedyczak F, Szcześniak P (2009) Modelling and analysis of matrix-reactance frequency converters using voltage source matrix converter and LF transfer matrix modulation method. Przegląd Elektrotechniczny (Electr Rev) 2:125–130
4. Korotyeyev I, Fedyczak Z (2008) Steady and transient states modelling methods of matrix-reactance frequency converter with buck-boost topology. COMPEL: Int J Comput Math Electr Electron Eng 28(3):626–638
5. Korotyeyev I, Fedyczak Z, Szcześniak P (2008) Steady and transient state analysis of a matrix-reactance frequency converter based on a boost PWM AC matrix-reactance chopper. In: Proceedings of the international school on nonsinusoidal currents and compensation, ISNCC'08, Łagów, Poland (CD-ROM)
6. Szczęsny R (1999) Computer simulation of power electronic systems, (Komputerowa symulacja układów energoelektronicznych) (in Polish). Wydawnictwo Politechniki Gdańskiej, Gdańsk
7. Szcześniak, P (2010) Analiza i badania właściwości układu napędowego z matrycowo reaktancyjnym przemiennikiem częstotliwości o modulacji Venturiniego (in Polish). Przegląd Elektrotechniczny (Electr Rev), 6:155–158
8. Szcześniak P (2009) Analysis and testing matrix-reactance frequency converters. PhD thesis (in Polish), University of Zielona Góra, Zielona Góra
9. Szcześniak P, Fedyczak Z, Klytta M (2008) Modelling and analysis of a matrix-reactance frequency converter based on buck-boost topology by DQ0 transformation. In: Proceedings of power electronics and motion control conference, EPE-PEMC'08, Poznań, Poland, pp 165–172
10. Szcześniak P, Fedyczak Z, Tadra G (2011) Modeling of the matrix-reactance frequency converters using SVM method (in Polish). In: Proceedings of Sterowanie w Energoelektronice i Napędzie Elektrycznym, SENE (2011) Łódź, Poland (CD-ROM)
11. Venturini M, Alesina A (1980) The generalized transformer: a new bi-directional sinusoidal waveform frequency converter with continuously adjustable input power factor. In: Proceedings of IEEE power electronics specialists conference PESC'80, pp 242–252